# Design, Microfabrication and Thermal Characterization of a Hotspot Cooler Testbed for Convective Boiling Experiments in Extreme-microgap with Integrated Micropin-fins

Xuchen Zhang[1], Mohamed H. Nasr[2], David C. Woodrum[2], Craig E. Green[2], Peter A. Kottke[2], Thomas E. Sarvey[1], Yogendra K. Joshi[2], Suresh K. Sitaraman[2], Andrei G. Fedorov[2], Muhannad S. Bakir[1]
[1]School of Electrical and Computer Engineering, [2]G. W. Woodruff School of Mechanical Engineering
Georgia Institute of Technology,
791 Atlantic Dr. NW.
Atlanta, GA, 30332
Email: xzhang96@gatech.edu

## ABSTRACT

In this work, we designed, fabricated and characterized a novel hotspot testbed to dissipate ultra-high power density by two-phase convective boiling of refrigerant in a microgap with integrated micropin-fins and isolation air trenches around resistance heaters. The 300 μm long, 200 μm wide, and 10 μm tall microgap with 4 μm diameter micropin-fins was batch micro-fabricated in silicon. The 40 μm wide and 180 μm deep isolation air trenches around the heater and a $SiO_2$ passivation layer were used to provide thermal isolation. The testbed dissipates a power density of up to 4.75 kW/cm$^2$ using R134a refrigerant as the coolant. Thermal resistance and pumping power were compared between the micropin-fin device of interest and a reference 'empty microgap' device to assess tradeoffs in performance. Micropin-fins were found to slightly reduce thermal resistance at the cost of a large increase in pumping power. In addition to experimental work, thermo-mechanical simulations were implemented to analyze the reliability of the device for high pressure conditions.

**KEY WORDS:** microfluidic cooling, high heat flux, two phase, heat sink, thermal testing, reliability.

## NOMENCLATURE

| | |
|---|---|
| $\alpha$ | the coefficient of thermal expansion (CTE) |
| E | modulus |
| G | mass flux |
| k | thermal conductivity |
| $\Delta P$ | pressure drop |
| $R''$ | thermal resistance |
| $T_f$ | inlet fluid temperature |
| $T_h$ | heater temperature |
| ν | Poisson's Ratio |

## INTRODUCTION

Driven by the rapidly increasing demand of high performance computing, the integration level and power density of electronics continue to increase, which subsequently necessities advances in cooling. Moreover, the non-uniform power dissipation in modern chips presents an additional challenge to the design of an effective cooling solution [1]. The temperature of the hotspot region, rather than the temperature of the background, often limits a chip's performance by locally driving temperature above operating limits and becoming the thermal design limiter [2]. Novel methods for cooling hotspots with high heat flux is required, and embedded microfluidic cooling is believed to be a promising solution [3] [4].

Forced convection in microchannels using both single phase and boiling (two-phase flow) has been widely explored for a number of decades. In 1981, Tuckerman and Pease [5] demonstrated single-phase microfluidic cooling for the first time using deionized (D.I.) water. By using microchannels (50 μm channel width, 50 μm wall width, and 302 μm height), they were able to dissipate a heat flux of 790 W/cm$^2$ with a maximum substrate temperature rise of 71 $^o$C. The heat transfer and pressure drop phenomena of micropin-fin heat sinks were investigated by Peles et al. [6]; the study concluded that cylindrical micropin-fin arrays are superior to plain microchannel based cooling. A three-tier single phase microfluidic cooled 3D IC stack was studied by Brunschwiler, et al. [7] with a footprint of 1 cm$^2$ and maximum power of 390 W.

Two-phase convective cooling in microgap coolers has a potential for hotspot mitigation as the low thermal resistance in the thin liquid layer covering the microgap surface was shown to offer ultra-high heat removal rate [8]. Prior studies of two-phase micro-coolers have shown the dissipation of heat fluxes up to 350 W/cm$^2$ [9-13]. Reeser et al. [9] recently compared the heat transfer and pressure drop characteristics of HFE-7200 and D.I. water in inline and staggered micropin-fin arrays with a height of 305 μm and diameter of 153 μm on a heated base area of 0.96 cm X 2.88 cm. Heat fluxes ranging from 1 to 36 W/cm$^2$ for HFE-7200 and 10 to 110 W/cm$^2$ for water were studied. Kim et al. [10] investigated 10 mm wide, 37 mm long micro-gap-channels; the channel height range was 110 μm to 500 μm and heat flux was 20 W/cm$^2$. Krishnamurthy et al. [11] dissipated heat fluxes up to 350 W/cm$^2$ with a 250 μm deep and 100 μm tall circular staggered micropin-fins using convective boiling of water at mass fluxes up to 794 kg/m$^2$s. Kosar et al. [12] dissipated up to 312 W/cm$^2$ with staggered hydrofoil based fins that are 243 μm tall and 150 μm apart with R123 as the working fluid at mass fluxes up to 2,349 kg/m$^2$s. Bowers et al. [13] dissipated heat fluxes up to 256 W/cm$^2$ with cylindrical microchannels of 510 μm diameter with R113 as the working fluid and volumetric flow rates up to 95 ml/min.

However, experiments of extreme-microgap with multi-kW/cm$^2$ heat fluxes have not been reported. In this work, a hotspot cooler testbed for convective boiling experiments in extreme-microgap with integrated micropin-fins was designed, fabricated and tested. The detailed fabrication technologies are presented. The maximum heat flux during testing was 4.75 kW/cm$^2$ with flow rates in the range of 0.1 – 0.3 ml/min. The thermal resistance and pressure drop of the device were characterized and compared with a reference device without

micropin-fins (Note: for the remainder of the paper, this device will be referred to as 'empty gap' device). A reduction in thermal resistance was observed with the surface enhancement of the micropin-fins. A tradeoff to this improved thermal performance is a large increase in pumping power resulting from the high constriction of fluid flow. In addition, the reliability analysis shows that the device can sustain 3000 kPa static pressure and 1000 kPa pressure drop across the microgap.

## DESIGN AND FABRICATION

The testbed consists of a 300 µm long, 200 µm wide and 10 µm tall microgap with 4 µm diameter in-line micropin-fins, as shown in Fig. 1 (a). In addition to fluid inlet and outlet ports, pressure ports are included on either side of the microgap in order to accurately measure pressure drop across the microgap while excluding pressure drop due to rapid flow constriction/expansion at the inlet and outlet ports [4]. One serpentine thin-film platinum heater and six resistance temperature detectors (RTDs) are deposited on the silicon to deliver high heat fluxes and perform accurate wall temperature monitoring, as shown in Fig. 1 (b). Next, 40 µm wide, 180 µm deep air trenches are etched around the heater to provide thermal isolation. A thin passivation layer of $SiO_2$ (~ 1 µm) is deposited on the heater and thermometry to further minimize thermal loss.

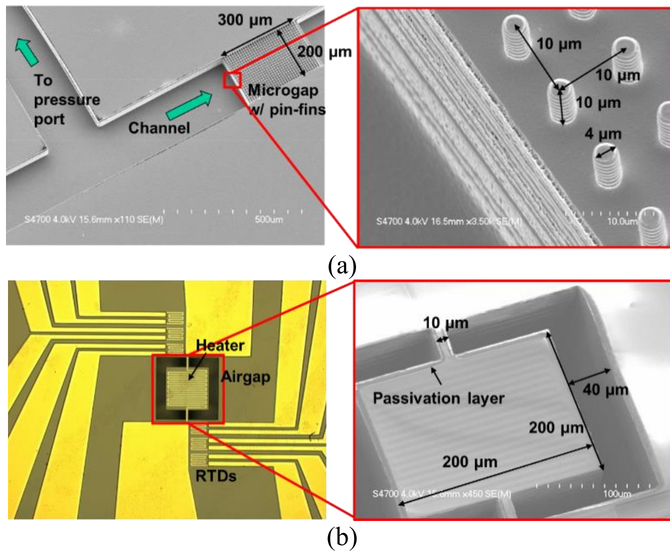


Fig. 1. Microgap side (a) and heater side (b) of the testbed

The fabrication process of the testbed is shown in Fig. 2. The process begins with a 280 µm thick double side polished wafer. A standard Bosch process with alternating of $SF_6$ (for etching) and $C_4F_8$ (for passivation) was used to create the 10 µm (± 0.5 µm) tall micropin-fins and the microgap. A second Bosch process was then used to etch the 50 µm (± 3 µm) deep channel. Next, the microgap was sealed using a pyrex cap with anodic bonding under the voltage of 800 V at 350 °C. The bonded wafer was then flipped and a 1 µm thick insulating silicon dioxide layer was deposited using low pressure chemical vapor deposition (LPCVD). The 200 nm (±5 nm) thick Platinum heater/RTDs and 500 nm (±10 nm) thick gold pads were then deposited on the $SiO_2$ layer. A second $SiO_2$ layer was deposited on the heater/RTDs as a passivation layer using LPCVD. The air trenches were then etched using Bosch process. Lastly, inlet, outlet, and pressure measurement ports were etched using the Bosch process from the same side of the wafer.

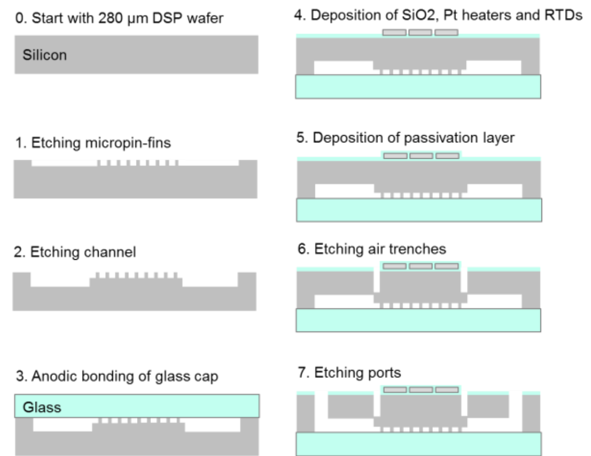


Fig. 2. Fabrication process

## THERMAL TESTING

### A. Testing Setup and Procedure

An overview of the experimental setup is presented in Fig. 3. The device is housed in a Polyether ether ketone (PEEK) package with machined O-ring groves for airtight sealing of the inlet/outlet ports and pressure taps. A cross-sectional view of the packaged device that makes up the test section is shown in Fig. 4. The pressure drop, heater resistance, circuit current, inlet/outlet fluid temperatures and fluid reservoir temperature were recorded with an Agilent 34970A data acquisition unit. A

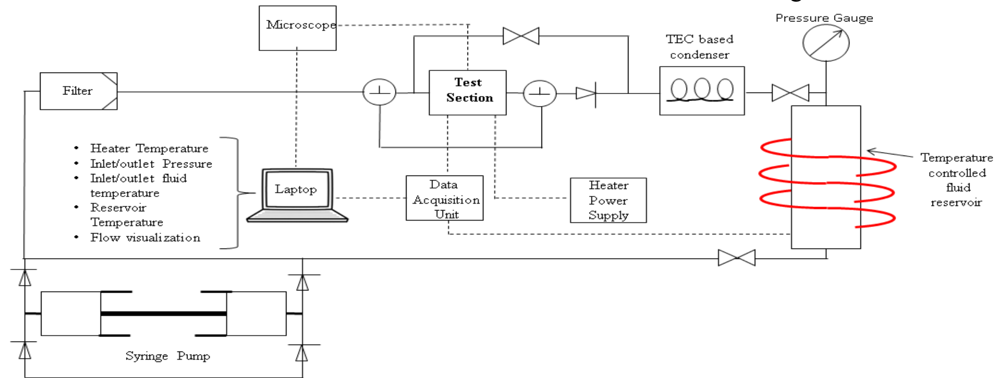


Fig. 3. Test Setup Schematic

KDS Scientific Legato 270 series syringe pump was used to drive refrigerant through the test section at the desired flow rate. The fluid temperature measurements were obtained with Omega K-type thermocouples. The pressure drop was measured with Omega PX 309 series pressure transducers. The power was supplied to the device heaters with an Agilent E3641A power source. A fan cooled WBA series thermoelectric was used to condense vapor exiting the test section. The reservoir tank was heated by electrical wire heaters with an Omega CN4000 PID controller to drive refrigerant into the system.

Linear correlation between the heater resistance and temperature was obtained before testing by calibrating test devices in a vacuum controlled oven. Experiments began by evacuating the experimental setup to remove air in the system followed by charging the test loop with R134a. The reservoir tank, filled with refrigerant, was pressurized with wire heaters to ensure complete filling of the experimental loop with liquid. R134a was pumped to the test section at 22.4 ºC inlet temperature with flow rates ranging from 0.1 – 0.3 ml/min. Power was applied to the heaters in 0.1-0.25 W increments until steady state temperatures and pressures were achieved. Power to the heaters was turned off when local dryout was observed in the microgap or when the inlet pressure was approaching glass syringe limits to avoid catastrophic failure.

The error of the K-type thermocouple used for heater calibration is +/- 0.9 °C, the error in power applied to the heaters from Agilent E3641A power source is +/- 0.011 W, the error in the mass flow rate from syringe pump is +/- 0.01 mL/s, and the error in the pressure transducer measurements is +/- 8.62 kPa. The error in microgap height, air trench depth, and micropin-fin height is within +/- 5% of the reported dimensions, and the error in the heater length and width is within +/- 1% of the reported dimensions. Error propagation was applied to assess the uncertainty in heat flux and thermal resistance which are found to be +/- 1.5% and +/- 1.7%, respectively. The average uncertainty of pumping power in the empty gap and micropin-fin devices is +/- 46.2 % and +/- 8.8 %, respectively. The lager uncertainty of pumping power in the empty gap device is due to the low pressure drop across the microgap which is comparable with the error in pressure measurements.

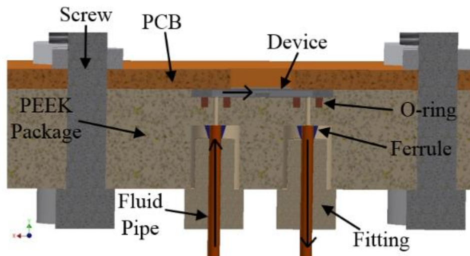


Fig. 4. Cross-sectional view of the test section with airtight packaging

## B. Results and Discussion

*Thermal resistance and pumping power*

The minimum overall thermal resistance after the onset of boiling in the microgap at each tested flow rate for devices with and without micropin-fins is shown in Fig. 5. The thermal resistance is calculated as,

$$R'' = \frac{T_h - T_f}{q''_h}, \quad (1)$$

where $T_h$ is the heater temperature, $T_f$ is the ambient air temperature outside the device, and $q''_h$ is the heat flux at the heater area, calculated as the ratio of the power input to the heater to heater surface area (200 µm x 200 µm).

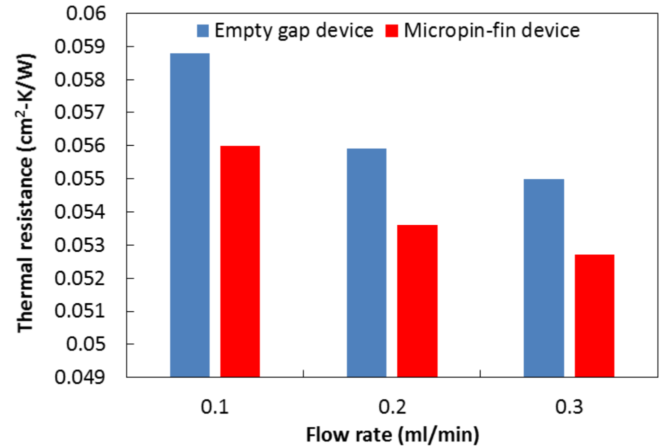


Fig. 5. Minimum thermal resistance after the onset of boiling vs flow rate comparing the micropin-fin device with the empty gap device without micropin-fins

The minimum thermal resistance of the micropin-fin device is slightly smaller than the empty gap device. Given that the surface area is enhanced by a factor of 2.27 in the micropin-fin device, it was expected that the thermal resistance would be reduced by approximately the same factor since it is inversely proportional to the surface area. However, in two phase convective boiling, the highest heat removal rate occurs when a continuous thin liquid film covers the microgap surface; the thinner the film, the higher the heat removal rate [14]. Although the micropin-fins increase surface area by a factor of 2.27, they have the unintended effect of breaking up the thin film that dominates convective boiling mechanism in microgaps of ultra-small gap height [14]. The combined effects of an increase in surface area and the existence of a thin film, although broken up, in the micropin-fin device reduce the thermal resistance beyond that of an empty microgap without micropin-fins for the same heater heat flux; however it is difficult to predict the reduction given the complexity associated with the physics of boiling. This is contrary to single phase convective cooling, where the effect of a surface area enhancement increase directly correlates to a reduction in thermal resistance by approximately the same factor.

The pumping power as a function of heat flux for the micropin-fin device and empty gap device are compared in Fig. 6. The volumetric flow rates were ranging from 0.1 ml/min to 0.3 ml/min in both devices. The volumetric flow rates were limited to 0.3 ml/min because maximum pressure at qualities approaching unity reached 2000 kPa, which is at the upper limit of glass syringes used to pump the fluid before catastrophic failure.

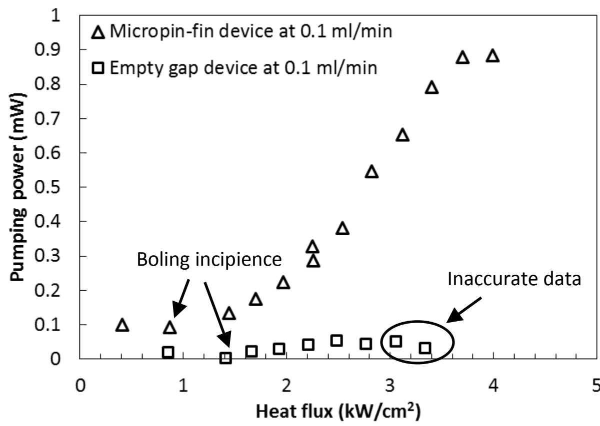

(a)

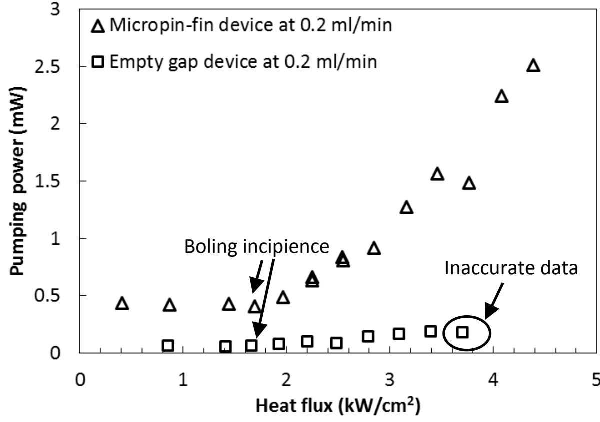

(b)

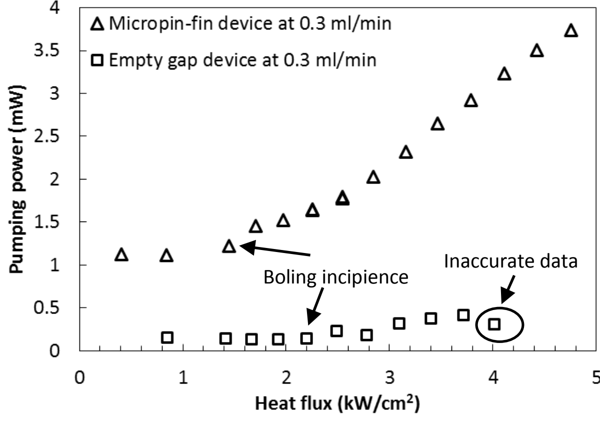

(c)

Fig. 6. Comparison of pumping power vs. heat flux between the micropin-fin device and empty gap device at flow rates of (a) 0.1 ml/min, (b) 0.2 ml/min and (c) 0.3 ml/min

In the single phase domain, pumping power is nearly constant with increased heat flux in both devices. The onset of boiling in the microgap that occurs with increases in applied heater heat flux causes an increase in pumping power due to the acceleration between liquid and vapor states as well as viscous losses. The last data points where pumping power decreased in the empty microgap device are not accurate representations of the actual two phase pressure drop in the microgap, but result from boiling incipience in the inlet plenum where the pressure tap is located. The pressure transducing element, located further away from the test section, detects saturation pressure at ambient temperature, which is lower than the saturation pressure at the inlet of the microgap. In micropin-fin device tests, the recorded pumping power accurately represents two-phase pressure drop across the microgap for all heat fluxes because boiling was not observed in the inlet plenum.

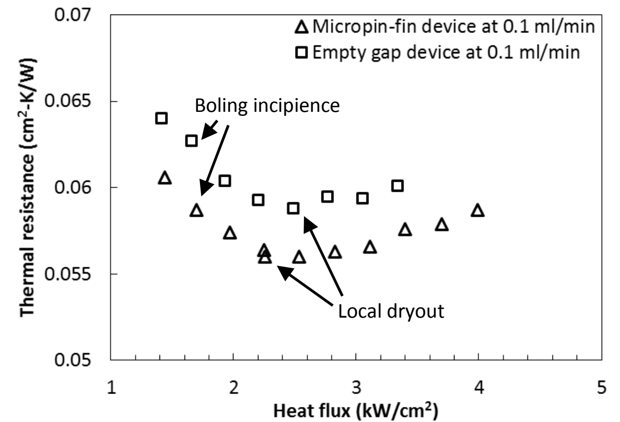

(a)

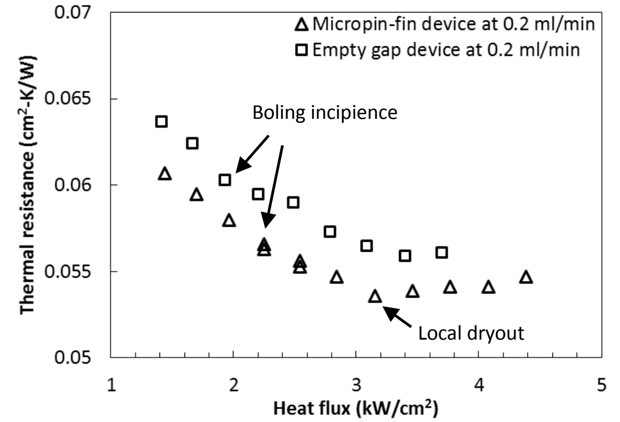

(b)

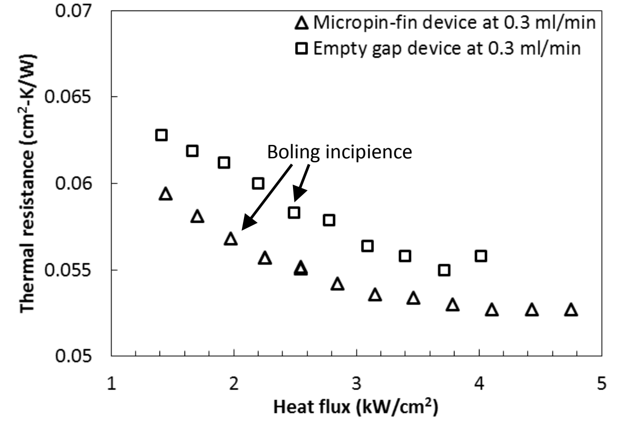

(c)

Fig. 7. Comparison of thermal resistance vs. heat flux between the micropin-fin device and empty gap device at flow rates of (a) 0.1 ml/min, (b) 0.2 ml/min and (c) 0.3 ml/min

The tight placement of micropin-fins (10 µm pitch) highly constricts fluid flow, increasing hydrodynamic resistance and

viscous losses thereby driving the pressure drop much higher than that of an empty gap. As a result, the pumping power in the micropin-fin devices is much higher than that of the empty gap devices for the flow rates investigated.

The comparison of thermal resistance as a function of heat flux between the micropin-fin device and empty gap device at various flow rates is shown in Fig. 7. In the single phase domain, a decrease of thermal resistance with respect to heat flux is observed. We believe this is due to an improvement in heat rejection of the device by natural convection to the ambient air. Detailed explanation can be found in [14]. Upon the onset of boiling, the thermal resistance continues to decrease with respect to heat flux due to convective boiling in the microgap prior to the onset of local dryout, which is evident for the empty gap device at 0.1 ml/min and the micropin-fin device at 0.1 ml/min and 0.2 ml/min. At the onset of local dryout, the continuous liquid layer covering the heated surface of the microgap boils away, leaving mostly dry area. Therefore, the thermal resistance increases as fluid available for heat removal is reduced. The local dryout is not observed in the 0.3 ml/min plot because the test did not go to high enough heat fluxes to reach local dryout. Heater degradation limits the maximum heat fluxes tested in these experiments.

Compared to the empty gap device, the thermal resistance of the micropin-fin device has an average reduction of 3.5% due to the surface area enhancement. However, the cost associated with the very large increase in pumping requirement does not justify the integration of micropin-fins for the dimensions studied. Although the empty gap device, which only exploits the high heat removal rates of thin film convective boiling, was more efficient than the micropin-fin enhanced device, there may be other configurations of micropin-fins (e.g. larger spacing) that reduce the pressure drop to the point where an optimization of micropin-fin surface enhancement and the pumping requirement can be achieved.

*Heat spreading*

One of the main challenges in conducting a study on ultra-small microgaps of 10 µm height (to accurately extract thermal data that represents the boiling phenomenon occurring within the microgap) is spreading of the power applied at the heaters away from the microgap test section of interest. The 270 µm thick silicon base separating the heaters and the fluid within the microgap constitutes a major path for heat flow to bypass the microgap, as shown in Fig. 8 (a). Furthermore, the power input required to generate ultra-high heat fluxes (4.75 kW/cm$^2$) at the small heater surface area (200 µm x 200 µm) is very low (1.9 W); this adds to the design challenge because even small amounts of heat dissipation away from the microgap make up a significant portion of the total input power. The air trenches implemented in the design to overcome these challenges help streamline the heat flow originating at the heaters to the microgap, as shown in Fig. 8 (b). The clear transitions in thermal resistance and pumping power trends, which correspond to distinct flow regimes in Fig. 6 and Fig. 7, show that the thermal data correlates to convective boiling in the microgap. Still, there are non-negligible heat losses due to conduction spreading through the 10 µm wide bridges that connect the heater to the bulk silicon and provide mechanical support for the heater, as shown in Fig. 1 (b). Quantitative modeling of the heat loss will be analyzed in the near future.

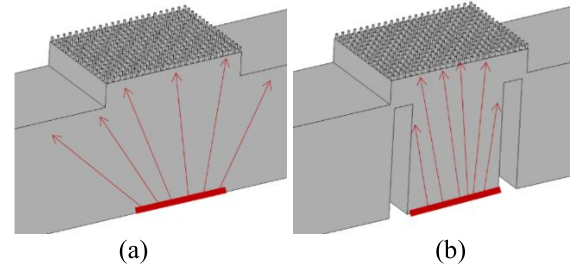


Fig. 8. Air trenches isolation effect on heat spreading: (a) without air trenches, heat generated at the heaters spreads through the device by conduction; (b) with air trenches, heat flow is streamlined to the microgap

## RELIABILITY MODELING

The successful implementation of this on-chip microfluidic cooling architecture requires the effective use of all aspects of co-design including electrical, thermal, fluidic, and mechanical aspects. Reliability modeling is conducted to assess the impact of the anticipated fluidic pressure loads on system integrity for high-performance operating conditions. ANSYS® Mechanical is used to develop the structural finite element model. The resulting stresses are examined and the potential for failure is evaluated for critical locations.

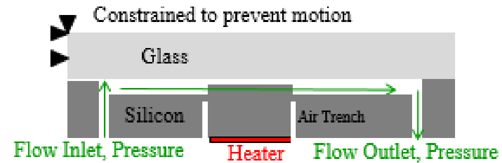


Fig. 9. Side view of hotspot geometry as modeled using ANSYS®

Table 1. Material Parameters

| Parameter | Silicon | Glass |
|---|---|---|
| Material Model | Elastic | Elastic |
| Modulus, E | 140 GPa | 70 GPa |
| Poisson's Ratio, ν | 0.28 | 0.16 |
| Conductivity, k | 139 W/mk | 1.14 W/mk |
| CTE, $\alpha$ | 2.6 e$^{-6}$/ºC | 3.8 e$^{-6}$/ºC |

The model geometry is constructed and meshed to accurately match the design architecture. The silicon substrate is modeled including the microchannel and microgap as well as the isolation air trenches surrounding the heaters. The glass cap is also modeled, and it is assumed to be perfectly bonded to the silicon substrate at all contact interfaces. The actual heaters themselves are not included as they have little to no effect on the structure as a whole. Fig. 9 illustrates the model's layout. The model's material properties are shown in Table 1.

This model is loaded with internal pressures according to the expected working conditions of the device. The high performance fluid typically flows through the internal microchannel at working pressures in excess of 2000 kPa. This value depends upon flow rate, heat flux, and temperature of the fluid. In this model, the pressure is assumed to be 3000 kPa at the inlet with negligible pressure loss until it reaches the

microgap. Within the microgap the pressure is assumed to linearly decay from 3000 kPa to 2000 kPa due to pressure drop as the fluid flows through the gap. The remainder of the channel is subjected to 2000 kPa static pressure. The model is also constrained at two nodes sufficiently far away from the critical regions of the geometry to prevent rigid body translation and rotation. The results of this simulation are shown in Fig. 10.

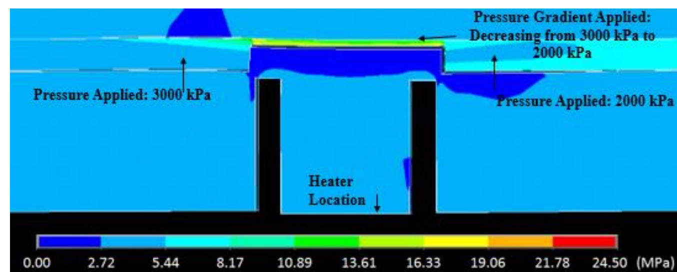

Fig. 10. First principal stress results for high pressure loading of 3000 kPa

For this pairing of brittle materials, first principal stress is chosen as the critical stress value. The microgap itself experiences the highest principal stress of 24 MPa due to the high pressure drop across that section. A defect or crack size of approximately 300 μm would be required for fracture of these materials at such a low principal stress as the fracture toughness of silicon and glass is 0.8 and 1.0 MPa$\sqrt{m}$, respectively [15]. The introduction of the isolation air trenches in this configuration has negligible effect on the reliability of the system from a structural standpoint. Further parametric analysis may be performed to examine the limits on etch depth and width of this air trenches.

## CONCLUSION AND FUTURE WORK

In this paper, a hotspot cooler testbed for convective boiling experiments in extreme-microgap with integrated micropin-fins and isolation air trenches was designed, fabricated and tested. The maximum heat flux during testing reached up to 4.75 kW/cm$^2$ with flow rates ranging from 0.1 – 0.3 ml/min. A reduction in thermal resistance of approximately 3.5% was observed with the surface enhancement of the micropin-fins with a tradeoff of a large increase in pumping power resulting from the high constriction of the fluid flow. In addition, the reliability analysis showed that the device can sustain 3000 kPa pressure and 1000 kPa pressure drop across the microgap. The thermal isolation air trenches reduced heat losses by conduction spreading through silicon between the heater and microgap and had negligible effect on the reliability of the system. Additional work includes quantitative characterization and modeling of the heat loss.


### Acknowledgments

The authors would like to thank DARPA ICECool Fundamentals Program for support of this work under contract number HR0011-13-2-0008.


### References


[1] M. Manno, et al., “Microcontact-Enhanced Thermoelectric Cooling of Ultrahigh Heat Flux Hotspots,” IEEE TCPMT, vol. 5, no. 12, pp. 1775–1783, Dec. 2015.

[2] H. Hamann et al., “Hotspot-limited microprocessors: direct temperature and power distribution measurements,” IEEE JSSC, vol. 42, no. 1, pp. 56–65, Jan. 2007.

[3] Y. Zhang, et al., “3-D stacked tier-specific microfluidic cooling for heterogeneous 3-D ICs,” IEEE TCPMT, vol. 3, no. 11, pp. 1811-1819, Oct. 2013.

[4] X. Zhang, et al., "3D IC with embedded microfluidic cooling: technology, thermal performance, and electrical implications," ASME InterPACKICNMM, San Francisco, CA, USA, July 2015.

[5] D. Tuckerman et al., “High-performance heat sinking for VLSI,” IEEE EDL vol. 2, no.5, pp. 126–129, May 1981.

[6] Y. Peles, et al., “Forced convective heat transfer across a pin fin micro heat sink,” Int. J. Heat Mass Transf., vol. 48, no.17, pp. 3615–3627, Aug. 2005.

[7] T. Brunschwiler, et al., “Validation of the porous-medium approach to model interlayer-cooled 3D-chip stacks,” IEEE 3DIC, pp. 1–10, San Francisco, CA, USA, Sep. 2009.

[8] A. Bar-Cohen, et al., “Modeling and prediction of two-phase microgap channel heat transfer characteristics,” Heat Transfer Engineering, vol. 30, no. 8, pp. 601-625, July 2009.

[9] A. Reeser, et al., “High quality flow boiling heat transfer and pressure drop in microgap pin fin arrays,” Int. J. Heat Mass Transf., vol. 78, pp. 974-985, Nov. 2014.

[10] D. Kim, et al., “Thermofluid characteristics of two-phase flow in micro-gap channels,” 11th IEEE I-THERM, pp. 979–992, Orlando, FL, USA, May 2008.

[11] S. Krishnamurthy, et al., “Flow boiling of water in a circular staggered micro-pin fin heat sink,” Int. J. Heat Mass Transf., vol. 51, no. 5, pp. 1349-1364, Mar. 2008.

[12] A. Koşar, et al., “Boiling heat transfer in a hydrofoil-based micro pin fin heat sink,” Int. J. Heat Mass Transf., vol. 50, no. 5, pp. 1018-1034, Mar. 2007.

[13] M. Bowers, et al., “High flux boiling in low flow rate, low pressure drop mini-channel and micro-channel heat sinks,” Int. J. Heat and Mass Transf., vol. 37, no. 2, pp. 321-332, Jan. 1994.

[14] M. Nasr, et al., “Extreme-Microgap (x-µgap) Based Hotspot Thermal Management with Refrigerant Flow Boiling”, 15th IEEE I-THERM, Las Vegas, NV, USA, May-June, 2016. (accepted)

[15] V. Hatty, et al., “Fracture toughness, fracture strength, and stress corrosion cracking of silicon dioxide thin films,” J. Microelectromechanical Systems, vol.17, no.4, pp. 943-947, Aug. 2008.